nature chemical biology

Article

https://doi.org/10.1038/s41589-022-01142-z

Structural basis of colibactin activation by the ClbP peptidase

Supplementary Information

Structural basis of colibactin activation by the ClbP peptidase

José A. Velilla[1], Matthew R. Volpe[2], Grace E. Kenney[2], Richard M. Walsh Jr[3,4], Emily P. Balskus[2,5], and Rachelle Gaudet[1]

Affiliations

1 Department of Molecular and Cellular Biology, Harvard University, Cambridge, MA USA

2 Department of Chemistry and Chemical Biology, Harvard University, Cambridge, MA USA

3 The Harvard Cryo-EM Center for Structural Biology, Harvard Medical School, Boston, MA

4 Department of Biological Chemistry and Molecular Pharmacology, Blavatnik Institute, Harvard Medical School, Boston, MA

5 Howard Hughes Medical Institute, Harvard University, Cambridge, MA USA

This file contains:

- Supplementary Table 1. Data collection and refinement statistics (molecular replacement)
- Supplementary Table 2. List of primers used for site-directed mutagenesis
- Supplementary Table 3. Cryo-EM data collection, refinement, and validation statistics
- Supplementary Figure 1. Structure of full-length ClbP
- Supplementary Figure 2. Sample biosynthetic gene clusters
- Supplementary Figure 3. Alignment of representative homologs
- Supplementary Figure 4. ClbP is the only prodrug-activating peptidase proposed to process a pseudodimeric substrate
- Supplementary Figure 5. Docking experiments to model precolibactin binding to ClbP
- Supplementary Note (Synthesis and validation of compound 1)

Additional Supplementary Data provided separately is a zip file containing:

- README.txt file
- Sequence similarity network for PF00144 family members in the correct size range and with at least two transmembrane domains (.cys file)
- Metadata file for sequences in the sequence similarity network (.xlsx file)
- Clustal Omega alignment for sequences from all representative nodes (.fa file)
- Clustal Omega alignment for sequences from all prodrug peptidase representative nodes (.fa file)
- Clustal Omega alignment for sequences from all ClbP representative nodes (.fa file)
- Clustal Omega alignment for all S12 sequences used in phylogenetic analyses (.fa file)
- Phylogenetic tree for S12 family members with available structures (.nwk file)

Supplementary Table 1. Data collection and refinement statistics (molecular replacement)

	Product-bound S95A-L454M-I478M (PDB: 7MDF)	Monoolein-bound S95A-L454M-I478M (SeMet) (PDB: 7MDE)
Data collection		
Space group	P 4_2 2_1 2	P 4_2 2_1 2
Cell dimensions		
a, b, c (Å)	96.69, 96.69, 182.74	97.47, 97.47, 183.97
α, β, γ (°)	90, 90, 90	90, 90, 90
Resolution (Å)	46.74 - 2.3 (2.38 - 2.3)	48.74 - 2.7 (2.8 - 2.7)
Total reflections	673835 (61048)	163298 (16722)
Unique reflections	39268 (3829)	25099 (2449)
I / σI	8.89 (1.32)	7.74 (1.22)
R_{sym} or R_{merge}	0.362 (2.781)	0.211 (1.338)
R_{meas}	0.3731 (2.872)	0.2294 (1.447)
CC1/2	0.997 (0.697)	0.994 (0.67)
Completeness (%)	99.81 (99.63)	99.79 (99.96)
Redundancy	17.2 (15.9)	6.5 (6.8)
Wilson B-factor	33.75	48.7
Refinement		
Resolution (Å)	46.74 - 2.3 (2.38 - 2.3)	48.74 - 2.7 (2.8 - 2.7)
No. reflections	39236 (3819)	25074 (2448)
No. reflections in R_{free}	1964 (190)	751 (74)
R_{work} / R_{free}	0.1914 / 0.2190	0.1948 / 0.2350
No. atoms	3935	3605
Protein	3431	3341
Ligand/ion	195	86
Water	309	178
B-factors		
Protein	56.56	67.5
Ligand/ion	83.66	76.18
Water	50.09	56.67
R.m.s. deviations		
Bond lengths (Å)	0.007	0.007
Bond angles (°)	0.89	0.92
Ramachandran plot		
Favored (%)	96.21	96.61
Allowed (%)	3.79	3.39
Disallowed (%)	0	0
Rotamer outliers (%)	2.59	2.98
Clashscore	8.33	4.85

Values in parentheses are for highest-resolution shell. Data for the product-bound structure merge reflections from 2 crystals. Data for the monoolein-bound structure were obtained from a single crystal.

Supplementary table 2. **List of primers used for site-directed mutagenesis**

Primer Name	Sequence
ClbP Add His FWD	CCACCATCACCATCACTGAGATCCGGCTGCTAACAAAGCCCGAAAG
ClbP Add His REV	CTCAGTGATGGTGATGGTGGTGGTGGTGGTGCTCGAGCTC
E92Q FWD	GTTTACCAGCTGGGATCGATGAGTAAGGCGTTTAC
E92Q REV	CAGCTGGTAAACTGTGTCTAGAGTATTCGCTTTCTGAC
S95A FWD	GGGAGCGATGAGTAAGGCGTTTACCGGACTTG
S95A REV	CATCGCTCCCAGCTCGTAAACTGTGTCTAGAG
S188A FWD	CTATGCCGCCGCCAATTATGATGTGTTGGGCG
S188A REV	GCGGCGGCATAGCTAAACTTCGCACCCG
S188N FWD	CTATGCCAACGCCAATTATGATGTGTTGGGCGCGGTG
S188N REV	GGCGTTGGCATAGCTAAACTTCGCACCCGGCG
K240A FWD	CTATGCACTGGGATTCGGCAAACCCGTTCTGTTTCATGC
K240A REV	CCAGTGCATAGCCGCTTGCCTTGTTGACAATAATCTCATCC
F243A FWD	CTGGGAGCCGGCAAACCCGTTCTGTTTCATGCG
F243A REV	TGCCGGCTCCCAGTTTATAGCCGCTTGCCTTGTTGAC
H257A FWD	GGAACGCTGTTCCTGCCGCCTATATCCATAGCACTC
H257A REV	GAACAGCGTTCCGGGCCAGAGGCGCATGAAAC
R308A FWD	GACAATGCTATCCTCTATGCCAGCGGTTGGTTTATCGACCAG
R308A REV	GAGGATAGCATTGTCTGCGGCAAGCGGAACATCACTATTACC
R308E FWD	CAATGAGATCCTCTATGCCAGCGGTTGGTTTATCGACCAGAATC
R308E REV	GAGGATCTCATTGTCTGCGGCAAGCGGAACATCACTATTACC
N331A FWD	GGGCAGGCTCCAAACTTTTCTTCTTGCATTGCGTTGCG
N331A REV	GTTTGGAGCCTGCCCACCGTGACTGATGTAAGGG
Y324A FWD	GCCCTGCCATCAGTCACGGTGGGCAGAATCCAAAC
Y324A REV	CTGATGGCAGGGCCTTGATTCTGGTCGATAAACCAACCG
D367A FWD	GGATATCGCTAATTATCTGCGCATTGGCAAATATGCTGAC
D367A REV	GATAATTAGCGATATCCGCGCAAAGCTGTAGTATCAGATTC
K374E FWD	GGCGAATATGCTGACGGCGCTGGTGATGCAATTAC
K374E REV	CCGTCAGCATATTCGCCAATGCGCAGATAATTATCGATATC
W460A FWD	CTTGACGCGCGTTTTATCTTGGTATGGGGTCCATCGAG
W460A REV	AACGCGCGTCAAGTCCTGGAGATAGTATACCCGGTGC
F462A FWD	GGCGTGCTATCTTGGTATGGGGTCCATCGAGCG
F462A REV	CAAGATAGCACGCCAGTCAAGTCCTGGAGATAGTATACC
W466A FWD	GGTAGCGGGTCCATCGAGCGTGTTGGCGATAC
W466A REV	GGACCCGCTACCAAGATAAAACGCCAGTCAAGTCCTGG

Supplementary Table 3. Cryo-EM data collection, refinement, and validation statistics

	WT ClbP (EMD-26593) (PDB: 7UL6)
Data collection and processing	
Magnification	60606
Voltage (kV)	300
Electron exposure (e–/Å^2)	76.191
Defocus range (μm)	0.8, 2.2
Pixel size (Å)	0.825
Symmetry imposed	C2
Initial particle images (no.)	562462
Final particle images (no.)	109906
Map resolution (Å)	3.73
FSC threshold	0.143
Map resolution range (Å)	3.20 – 5.53
Refinement	
Initial model used (PDB code)	7MDF
Model resolution (Å)	4.0
FSC threshold	0.5
Map sharpening *B* factor (Å^2)	188.1
Model composition	
Non-hydrogen atoms	6654
Protein residues	878
B factors (Å^2)	
Protein	58.0
Ligand	N/A
R.m.s. deviations	
Bond lengths (Å)	0.003
Bond angles (°)	0.615
Validation	
MolProbity score	1.32
Clashscore	5.13
Poor rotamers (%)	0.15
Ramachandran plot	
Favored (%)	97.81
Allowed (%)	2.19
Disallowed (%)	0

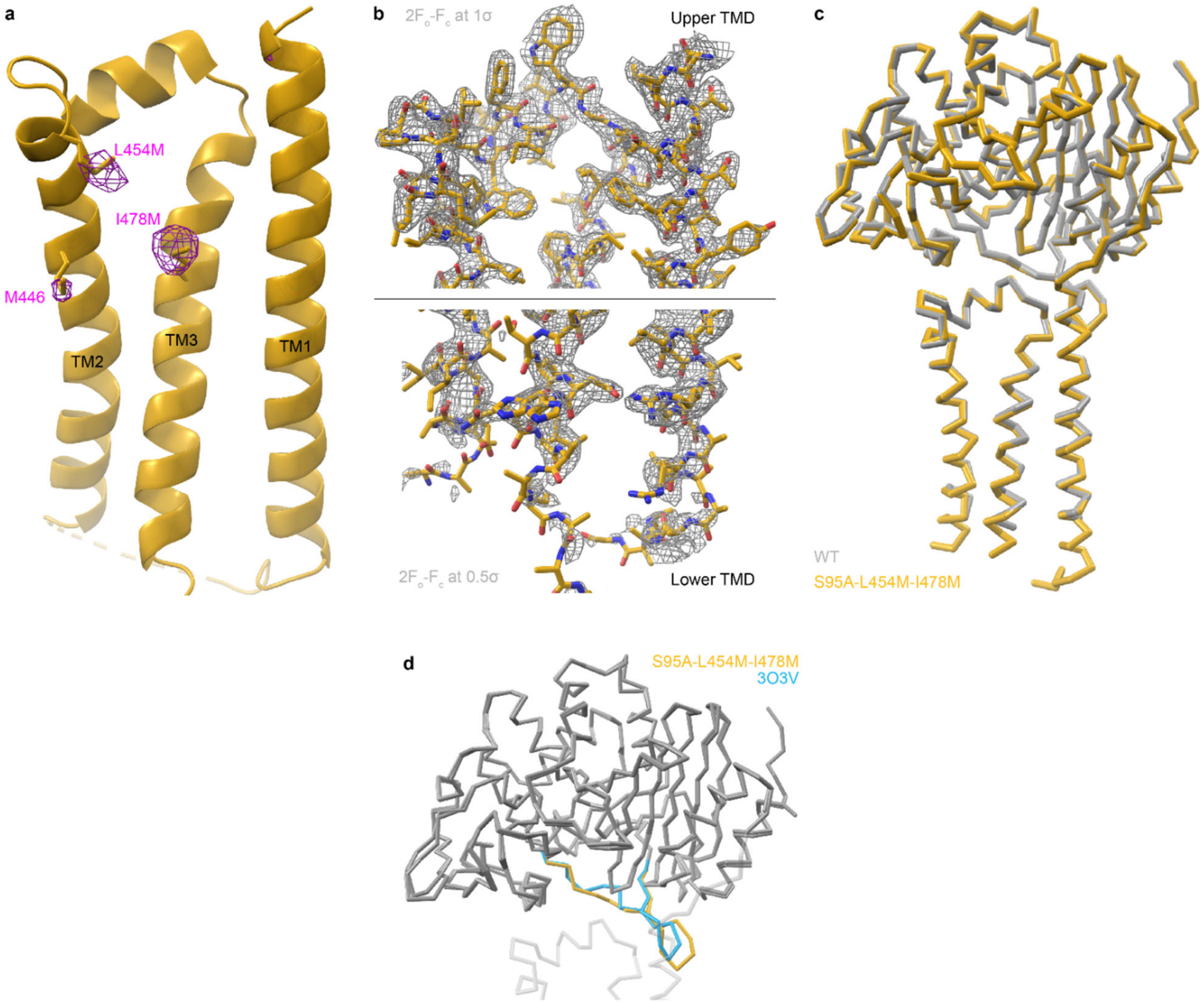

Supplementary Figure 1. Structure of full-length ClbP

a, Peaks from an anomalous difference Fourier map calculated from SeMet-substituted crystals match the positions of the methionines in the TMD and confirm the registry of our model (map contoured at 3σ). **b**, Sample $2F_o$-F_c maps show that parts of the TMD more proximal to the periplasmic domain (upper TMD) are better resolved than parts closer to the cytoplasm (lower TMD). **c**, Superposition of the structures for product-bound S95A-L454M-I478M (yellow) and wildtype ClbP (gray; companion paper[1]) showing that the two structures are nearly identical and that the introduced methionines do not affect the overall fold of the protein (RMSD = 0.37 over 436 shared Cα atoms). **d**, The periplasmic domain in our full-length structure is virtually identical to the structure of the isolated periplasmic domain published previously (PDB ID: 3O3V; RMSD 0.33 Å over 288 Cα atoms). The superposition of the two structures highlights differences in position of the β3-β4 loop (colored yellow in the product-bound S95A-L454M-I478M structure and cyan in the isolated periplasmic domain structure).

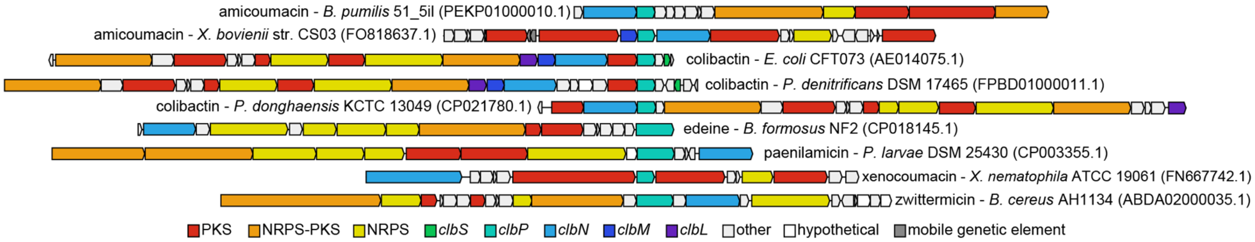
amicoumacin - B. pumilis 51_5il (PEKP01000010.1)
amicoumacin - X. bovienii str. CS03 (FO818637.1)
colibactin - E. coli CFT073 (AE014075.1)
colibactin - P. denitrificans DSM 17465 (FPBD01000011.1)
colibactin - P. donghaensis KCTC 13049 (CP021780.1)
edeine - B. formosus NF2 (CP018145.1)
paenilamicin - P. larvae DSM 25430 (CP003355.1)
xenocoumacin - X. nematophila ATCC 19061 (FN667742.1)
zwittermicin - B. cereus AH1134 (ABDA02000035.1)
🟥PKS 🟧NRPS-PKS 🟨NRPS 🟩clbS 🟩clbP 🟦clbN 🟦clbM 🟪clbL □other □hypothetical ■mobile genetic element

Supplementary Figure 2. Sample biosynthetic gene clusters

Biosynthetic gene clusters (BGCs) for natural products that utilize ClbN/ClbP systems for prodrug biosynthesis and prodrug removal, including amicoumacin[2,3], colibactin[4-6], paenilamicin[7], xenocoumacin[8], and zwittermicin[9,10]. While not previously identified as such, analysis of the edeine biosynthetic gene cluster[11-13] indicates that EdeA is likely also a true prodrug peptidase; we predict that EdeP is responsible for the biosynthesis of a previously unidentified acyl-D-Asn prodrug moiety (based on a condensation domain with homology to equivalent modules from surfactin, lichenysin, and colibactin; an adenylation domain predicted to have specificity for Asn; and an epimerase domain, required to produce D-Asn), as opposed to acting on 2,6-diamino-7-hydroxyazaleic acid as previously proposed[12]. In support of this, work in an accompanying paper uses a ClbP inhibitor to enrich several putative preedeines with colibactin-like prodrug moieties[1]. Additionally, a previously unidentified set of *clb*-like gene clusters are found in a subset of *Paenibacillus* species. These exhibit more genomic rearrangement than the *clb* clusters found in *Pseudovibrio* strains[61], and lack genes encoding ClbM and ClbS homologs, although a ClbL-like amidase is present, suggesting that formation of a colibactin pseudodimer is still plausible.

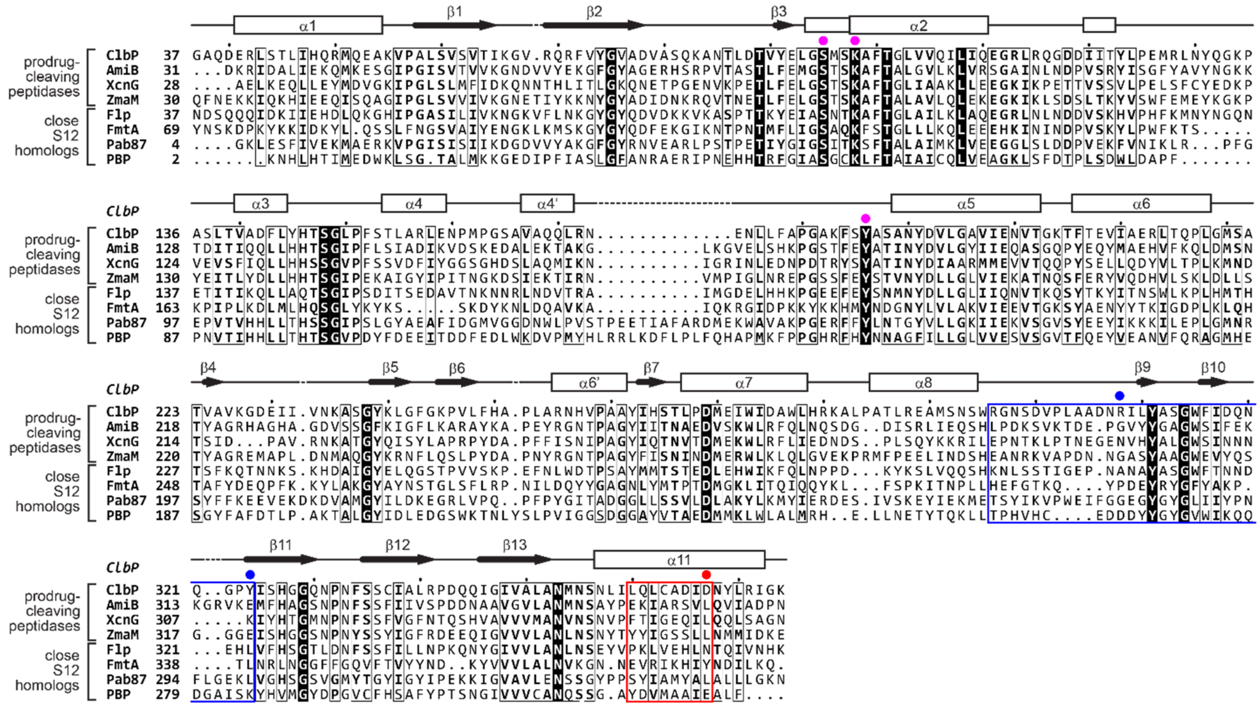
α1
β1
β2
β3
α2
prodrug-cleaving peptidases
close S12 homologs
ClbP 37 GAQDERLSTLIHQRMQEAKVPALSVSVTIKGV.RQRFVYGVADVASQKANTLDTVYELGSMSKAFTGLVVQILIQEGRLRQGDDIITYLPEMRLNYQGKP
AmiB 31 ...DKRIDALIEKQMKESGIPGISVTVVKGNDVVYEKGFGYAGERHSRPVTASTLFEMGSTSKAFTALGVLKLVRSGAINLNDPVSRYISGFYAVYNGKK
XcnG 28 ....AELKEQLLEYMDVGKIPGLSLMFIDKQNNTHLITLGKQNETPGENVKPETLFELGSTSKAFTGLIAAKLLEEGKIKPETTVSSVLPELSFCYEDKP
ZmaM 30 QFNEKKIQKHIEEQISQAGIPGLSVVIVKGNETIYKKNYGYADIDNKRQVTNETLFELGSTSKAFTALAVLQLEKEGKIKLSDSLTKYVSWFEMEYKGKP
Flp 37 NDSQQQIDKIIEHDLQKGHIPGASILIVKNGKVFLNKGYGYQDVDKKVKASPTTKYEIASNTKAFTGLAILKLAQEGRLNLNDDVSKHVPHFKMNYNGQN
FmtA 69 YNSKDPKYKKIDKYL.QSSLFNGSVAIYENGKLKMSKGYGYQDFEKGIKNTPNTMFLIGSAQKFSTGLLLKQLEEEHKININDPVSKYLPWFKTS.....
Pab87 4 ....GKLESFIVEKMAERKVPGISISIIKDGDVVYAKGFGYRNVEARLPSTPETIYGIGSITKSFTALAIMKLVEEGGLSLDDPVEKFVNIKLR...PFG
PBP 2 .......KNHLHTIMEDWKLSG.TALMKKGEDIPFIASLGFANRAERIPNEHHTRFGIASGCKLFTAIAICQLVEAGKLSFDTPLSDWLDAPF.......
ClbP
α3
α4
α4'
α5
α6
ClbP 136 ASLTVADFLYHTSGLPFSTLARLENPMPGSAVAQQLRN.............ENLLFAPGAKFSYASANYDVLGAVIENVTGKTFTEVIAERLTQPLGMSA
AmiB 128 TDITIQQLLHHTSGIPFLSIADIKVDSKEDALEKTAKG..........LKGVELSHKPGSTFEYATINYDVLGYIIEQASGQPYEQYMAEHVFKQLDMSN
XcnG 124 VEVSFIQLLHHSSGVPFSSVDFIYGGSGHDSLAQMIKN..........IGRINLEDNPDTRYSYATINYDIAARMMEVVTQQPYSELLQDYVLTPLKMND
ZmaM 130 YEITLYDLLHHTSGIPEKAIGYIPITNGKDSIEKTIRN..........VMPIGLNREPGSSFEYSTVNYDLLGLVIEKATNQSFERYVQDHVLSKLDLLS
Flp 137 ETITIKQLLAQTSGIPSDITSEDAVTNKNNRLNDVTRA..........IMGDELHHKPGEEFEYSNMNYDLLGLIIQNVTKQSYTKYITNSWLKPLHMTH
FmtA 163 KPIPLKDLMLHQSGLYKYKS.....SKDYKNLDQAVKA..........IQKRGIDPKKYKKHMYNDGNYLVLAKVIEEVTGKSYAENYYTKIGDPLKLQH
Pab87 97 EPVTVHHLLTHSSGIPSLGYAEAFIDGMVGGDNWLPVSTPEETIAFARDMEKWAVAKPGERFFYLNTGYVLLGKIIEKVSGVSYEEYIKKKILEPLGMNR
PBP 87 PNVTIHHLLTHTSGVPDYFDEEITDDFEDLWKDVPMYHLRRLKDFLPLFQHAPMKFPPGHRFHYNNAGFILLGLVVESVSGVTFQEYVEANVFQRAGMHE
ClbP
β4
β5
β6
α6'
β7
α7
α8
β9
β10
ClbP 223 TVAVKGDEII.VNKASGYKLGFGKPVLFHA.PLARNHVPAAYIHSTLPDMEIWIDAWLHRKALPATLREAMSNSWRGNSDVPLAADNRILYASGWFIDQN
AmiB 218 TYAGRHAGHA.GDVSSGFKIGFLKARAYKA.PEYRGNTPAGYIITNAEDVSKWLRFQLNQSDG..DISRLIEQSHLPDKSVKTDE.PGVYYGAGWSIFEK
XcnG 214 TSID...PAV.RNKATGYQISYLAPRPYDA.PFFISNIPAGYIQTNVTDMEKWLRFLIEDNDS..PLSQYKKRILEPNTKLPTNEGENVHYALGWSINNN
ZmaM 220 TYAGREMAPL.DNMAQGYKRNFLQSLPYDA.PNYRGNTPAGYFISNINDMERWLKLQLGVEKPRMFPEELINDSHEANRKVAPDN.NGASYAAGWEVYQS
Flp 227 TSFKQTNNKS.KHDAIGYELQGSTPVVSKP.EFNLWDTPSAYMMTSTEDLEHWIKFQLNPPD...KYKSLVQQSHKNLSSTIGEP.NANAYASGWFTNND
FmtA 248 TAFYDEQPFK.KYLAKGYAYNSTGLSFLRP.NILDQYYGAGNLYMTPTDMGKLITQIQQYKL...FSPKITNPLLHEFGTKQ....YPDEYRYGFYAKP.
Pab87 197 SYFFKEEVEKDKDVAMGYILDKEGRLVPQ..PFPYGITADGGLLSSVLDLAKYLKMYIERDES.IVSKEYIEKMETSYIKVPWEIFGGEGYGYGLIIYPN
PBP 187 SGYFAFDTLP.AKTALGYIDLEDGSWKTNLYSLPVIGGSDGGAYVTAEDMMKLWLALMRH..E.LLNETYTQKLLTPHVHC....EDDDYGYGVWIKQQ
ClbP
β11
β12
β13
α11
ClbP 321 Q..GPYISHGGQNPNFSSCIALRPDQQIGIVALANMNSNLILQLCADIDNYLRIGK
AmiB 313 KGRVKEMFHAGSNPNFSSFIIVSPDDNAAVGVLANMNSAYPEKIARSVLQVIADPN
XcnG 307 .....KIYHTGMNPNFSSFVGFNTQSHVAVVVMANVNSNVPFTIGEQILQQLSAGN
ZmaM 317 G..GGEISHGGSNPNYSSYIGFRDEEQIGVVVLANLNSNYTYYIGSSLLNMMIDKE
Flp 321 ...EHLVFHSGTLDNFSSFILLNPKQNYGIVVLANLNSEYVPKLVEHLNTQIVNHK
FmtA 338 ....TLNRLNGGFFGQVFTVYYND..KYVVVLALNVKGN.NEVRIKHIYNDILKQ.
Pab87 294 FLGEKLVGHSGSVGMYTGYIGYIPEKKIGVAVLENSSGYPPSYIAMYALALLLGKN
PBP 279 DGAISKYHVMGYDPGVCFHSAFYPTSNGIVVVCANQSSG.AYDVMAAIEALF....

Supplementary Figure 3. Alignment of representative homologs.

Alignment of representative prodrug-activating peptidase (top) and close S12 homologs with structures available (bottom; see Extended Data Fig. 9b). The blue and red boxes denote the secondary structures involved in dimerization detailed in Extended Data Fig. 9. Magenta dots mark the catalytic triad residues, red and blue dots the interface residues targeted for mutagenesis. The alignment shows a lack the primary sequence conservation of the ClbP dimerization interface among other prodrug-activating peptidases as well as among closely related S12 homologs with structures deposited in the PDB.

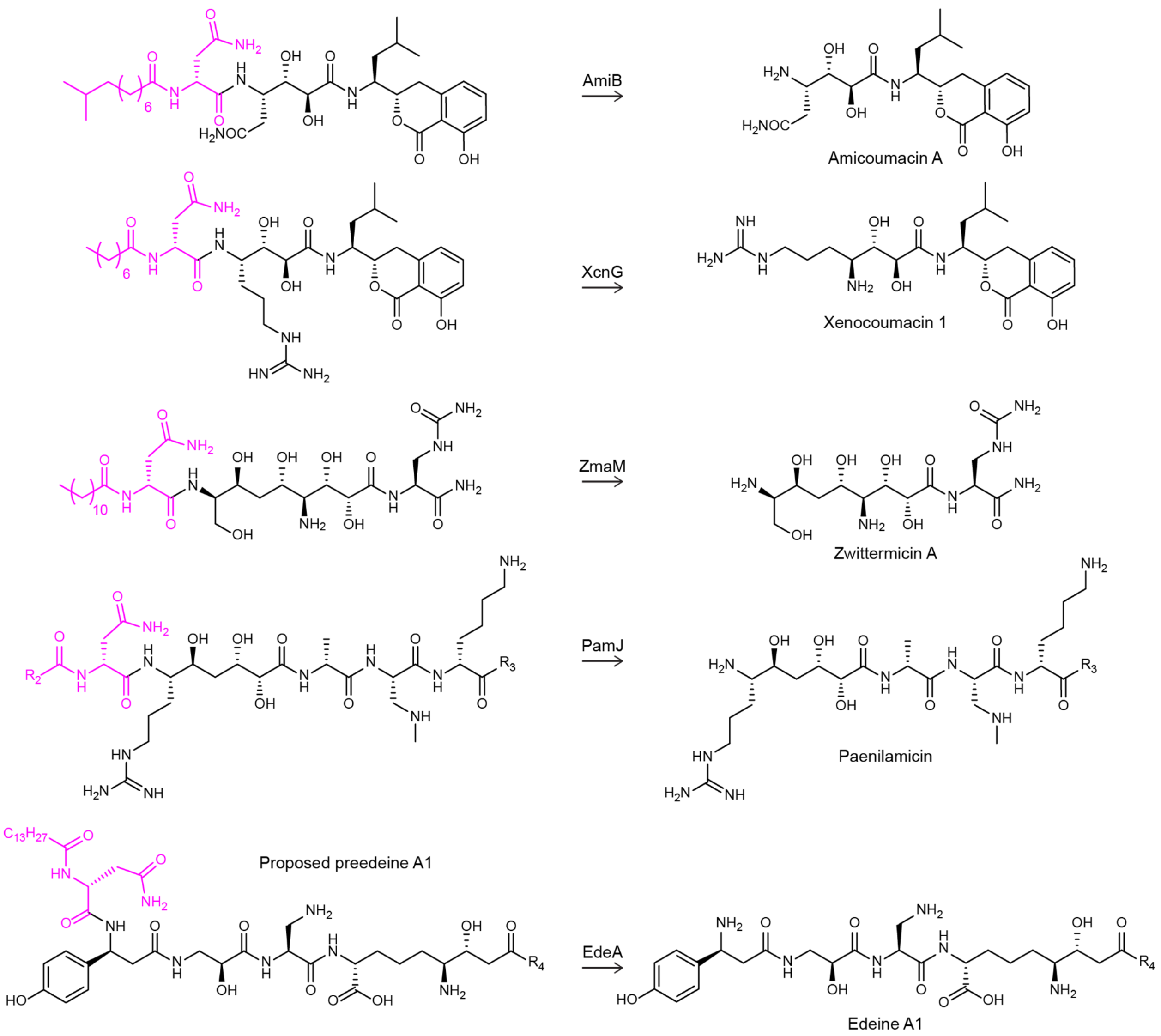

Supplementary Figure 4. ClbP is the only prodrug-activating peptidase proposed to process a pseudodimeric substrate

Chemical structure diagrams detailing the chemical reactions catalyzed by the amicoumacin[14], xenocoumacin[15], zwittermicin[9], and paenilamicin[16] peptidases—AmiB, XcnG, ZmaM, and PamJ respectively. Unlike ClbP, which is proposed to cleave a dimeric substrate (see Figure 1a), these peptidases are proposed to process monomeric precursors of their respective toxins. In all diagrams the *N*-acyl-D-asparagine prodrug motif cleaved from the precursor is colored in magenta. The R1 group in prezwittermicin represents a lauryl chain, as recently observed[1]. The R2 group in prepaenilamicin represents unknown acyl chains attached to their prodrug motifs, while the R3 in prepaenilamicin and paenilamicin represents a chemical structure derived from galantinic acid, *N*-methyl-diaminopropionic acid, glycine, and spermidine building blocks[16]. We further hypothesize that edeine biosynthesis employs a prodrug resistance mechanism and that EdeA is the activating peptidase. A proposed structure for a recently observed edeine A1 precursor containing a myristoyl-D-asparagine prodrug motif is shown[1], with R4 representing a glycylspermidine moiety[12].

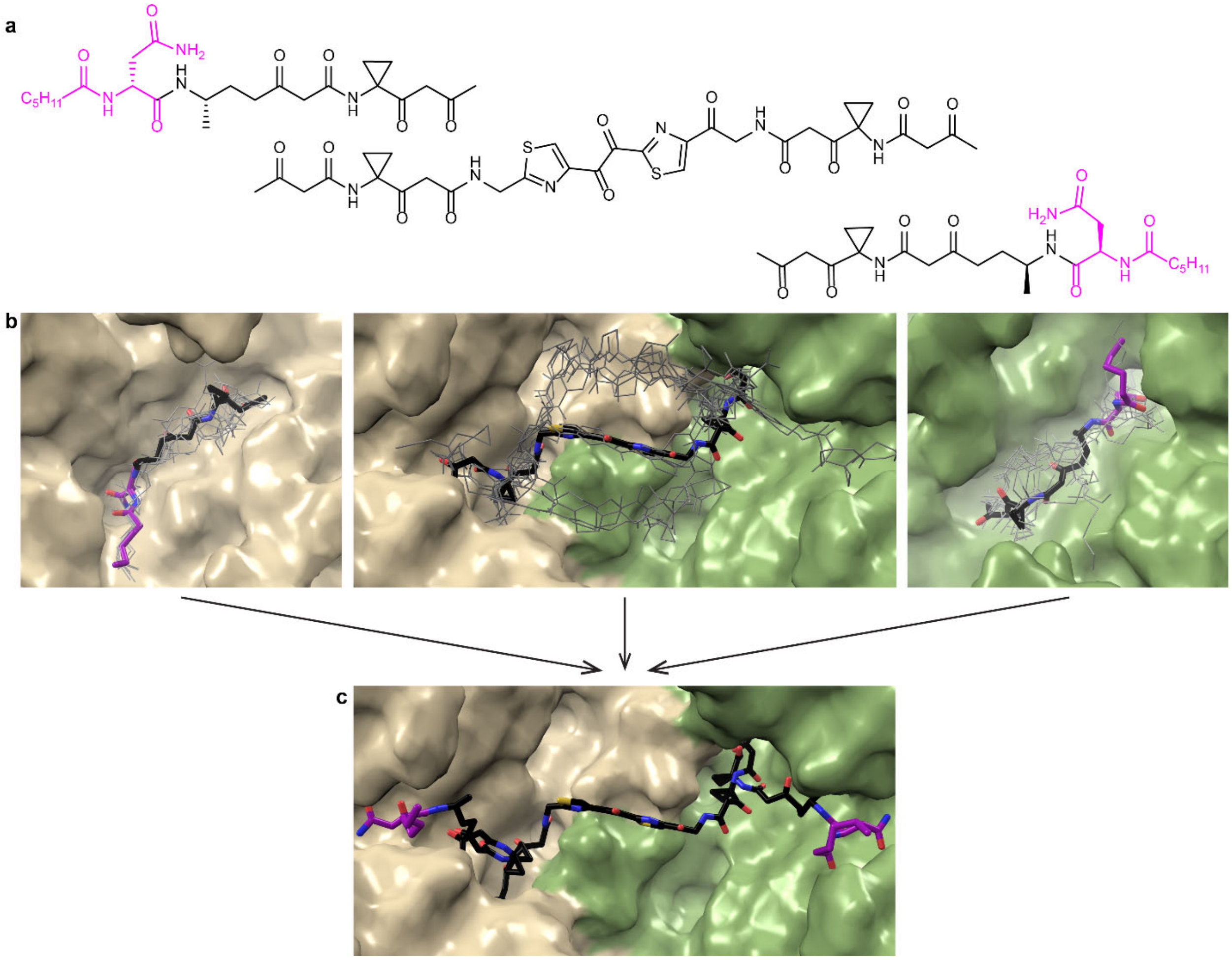

Supplementary Figure 5. Docking experiments to model precolibactin binding to ClbP

a, Chemical structure of the three overlapping fragments used to dock precolibactin onto the ClbP dimer. **b**, The panels show the selected pose (in sticks) for each of the three fragments along with alternative poses (gray lines). The selected pose for the two end fragments of precolibactin is shown with the nine other top scoring poses. Docking of the central fragment resulted in poses that either bound to a single subunit or that bridged both subunits. The selected pose for the central fragment is shown with other poses that bridge the two subunits and which reflect each of the three grooves that line the surface between the two active sites in dimeric ClbP. The selected pose for the central fragment was not among the top scoring poses, but it places the chemical groups that overlap with the two end fragments in proximity to their selected poses and therefore allowed us to connect the three fragments to generate a complete model of bound precolibactin. **c**, The selected pose for each of the three fragments are shown in the ClbP dimer cavity. Note that the docked molecules contain hexanoyl chains in place of the natural myristoyl chains.

Supplementary Note

Synthesis and validation of compound 1

NMR chemical shifts are reported in parts per million downfield from tetramethylsilane using the solvent resonance as internal standard for ^{1}H (DMSO-d_6 = 2.50 ppm) and ^{13}C (DMSO-d_6 = 39.52 ppm). Data are reported as follows: chemical shift, integration multiplicity (s = singlet, d = doublet, t = triplet, q = quartet, quint = quintet, m = multiplet), coupling constant, integration, and assignment. All solvents for synthesis were obtained from Sigma-Aldrich. All NMR solvents were purchased from Cambridge Isotope Laboratories (Tewksbury, MA). NMR spectra were collected in the Larkin-Purcell Instrumentation Center in Harvard University Department of Chemistry and Chemical Biology and visualized and processed using MestreNova, version 14.1.1-24571 (Mestrelab Research S.L., Escondido, CA). Preparative HPLC purification was run on a Dionex Ultimate 3000 instrument (Thermo Scientific) using Hypersil GOLDaQ column (250 mm x 20 mm, 5 μm particle size, Thermo Scientific).

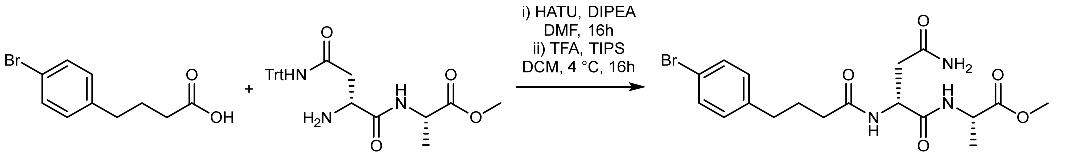

Compound **1**: In an oven-dried round-bottom flask, methyl *N*4-trityl-d-asparaginyl-l-alaninate (94 mg, 0.2 mmol, 1 equiv), 4-(4-bromophenyl)butanoic acid (59.7 mg, 0.24 mmol, 1.2 equiv), and 1-[Bis(dimethylamino)methylene]-1H-1,2,3-triazolo[4,5-b]pyridinium 3-oxide hexafluorophosphate (HATU, 93 mg, 0.24 mmol, 1.2 equiv) were dissolved in anhydrous dimethylformamide (DMF, 1.02 mL). Diisopropylethylamine (DIPEA, 89 mL, 0.51 mmol, 2.5 equiv) was added and the mixture stirred at room temperature overnight under a nitrogen atmosphere. The reaction mixture was then diluted with 10 mL 0.1N HCl and extracted with 10 mL ethyl acetate three times. The combined organic layers were washed with 5% lithium chloride, saturated sodium bicarbonate and saturated sodium chloride. The organic layer was then dried over anhydrous sodium sulfate and concentrated *in vacuo* to afford 132 mg white solid (94% crude yield). The crude intermediate was then immediately redissolved in DCM (3.8 mL) and cooled to 4°C. Triisopropylsilane (395 mL, 1.93 mmol, 10 equiv.) and trifluoroacetic acid (1.8 mL, 23 mmol, 120 equiv.) were added and the mixture stirred at 4°C overnight. The mixture was then concentrated *in vacuo* and the residue dissolved in DMSO and purified by preparative HPLC. The compound was eluted using the following gradient: 50% Solvent A for 2.5 minutes, gradient to 95% Solvent A over 7.5 minutes, hold at 95% Solvent A for 11.5 minutes, gradient to 50% solvent A over 1 minute, hold at 50% solvent A for 2.5 minutes (solvent A: HPLC-grade acetonitrile (VWR, HiPerSolv-Chromanorm) + 0.1% formic acid; solvent B: water + 0.1% formic acid; flow rate: 8 mL/minute; injection volume: 200 to 400 μL). The appropriate fractions were pooled and concentrated *in vacuo* to afford a white solid (30 mg, 33% yield over 2 steps). ^{1}H-NMR (500 MHz, DMSO-*d*$_6$): δ (ppm) = 8.10 (d, J = 7.3 Hz, 1H), 7.97 (d, J = 8.1 Hz, 1H), 7.49 – 7.42 (m, 2H), 7.26 (s, 1H), 7.19 – 7.12 (m, 2H), 6.86 (s, 1H), 4.60 (td, J = 8.1, 5.7 Hz, 1H), 4.25 (quint, J = 7.2 Hz, 1H), 3.60 (s, 3H), 2.54 (d, J = 7.6 Hz, 2H), 2.33 (dd, J = 15.3, 8.2 Hz, 1H)†, 2.11 (t, J = 7.4 Hz, 2H), 1.76 (quint, J = 7.5 Hz, 2H), 1.25 (d, J = 7.3 Hz, 3H). ^{13}C-NMR (126 MHz, DMSO-*d*$_6$): δ (ppm) = δ 173.3, 172.2, 171.7, 171.5, 141.8, 131.5, 131.2, 119.1, 52.3, 49.8, 48.0, 37.8, 34.9, 34.2, 27.2, 17.6. HRMS (ESI): calculated for $C_{18}H_{25}BrN_3O_5$ [M+H]$^+$, 442.0972; found 442.0969.

†A second peak matching this splitting pattern and integration (dd, J = 15.3, 8.2 Hz, 1H) appears at δ = 2.50 ppm in the ^{1}H-NMR, overlapping with the DMSO solvent residual peak. These peaks correspond to the two hydrogen atoms attached to the methylene carbon on the asparagine

sidechain. A ^{1}H-^{13}C HSQC was used to confirm the presence of the peak at 2.50 ppm and that these two peaks share an identical carbon coupling (see ^{1}H-^{13}C HSQC spectrum and inset below).

NMR spectra

Compound **1**: ^{1}H NMR (500 MHz DMSO-d$_6$)

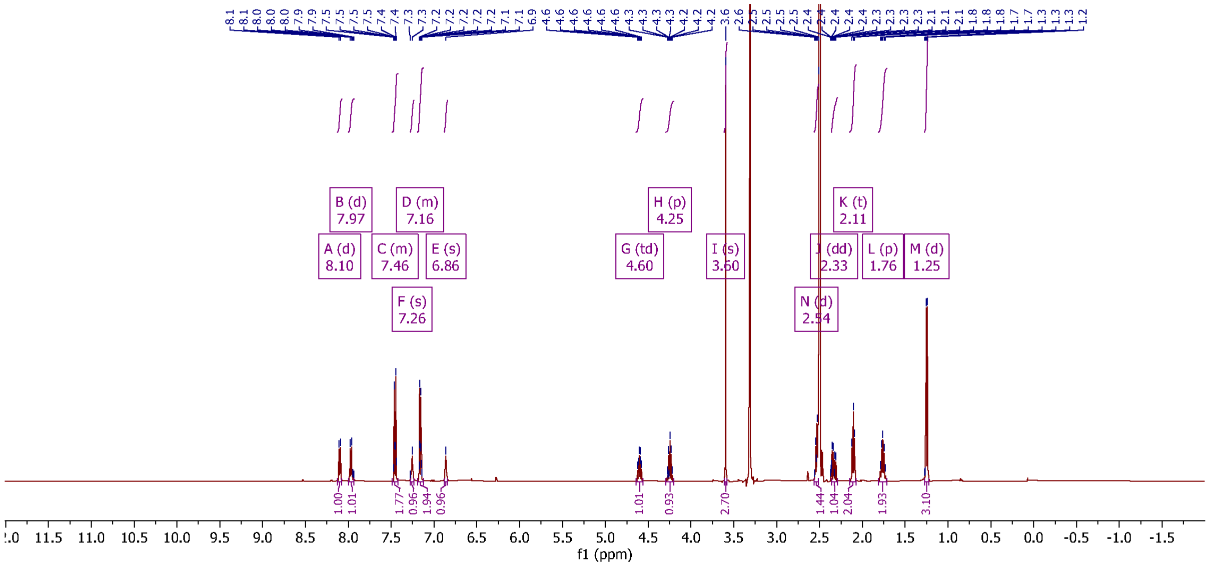

^{13}C NMR (126 MHz, DMSO-d$_6$)

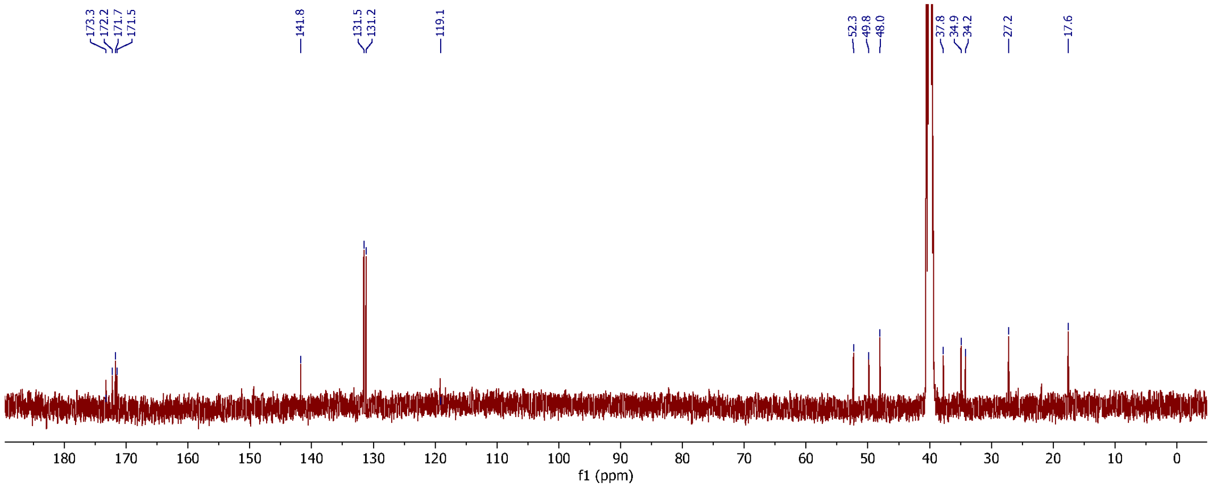

^{1}H-^{13}C HSQC (500 MHz, DMSO-d$_6$)

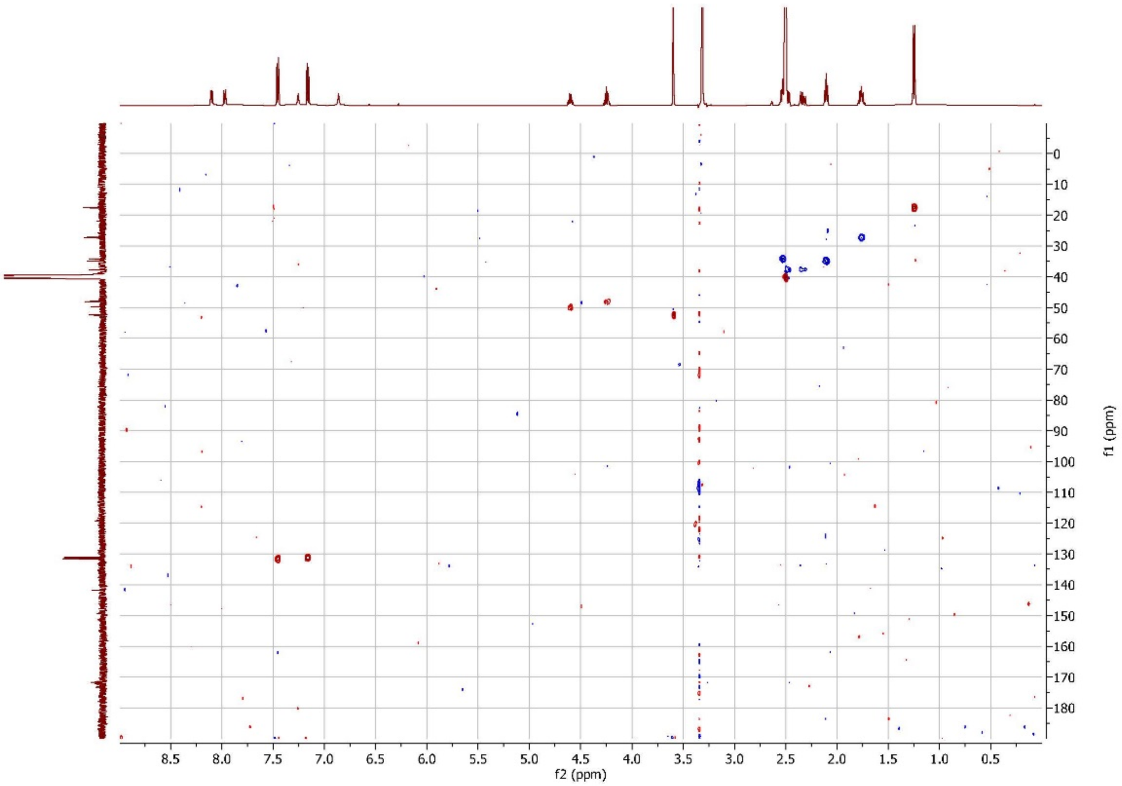

Inset focusing on the peaks corresponding to H-7 and H-19

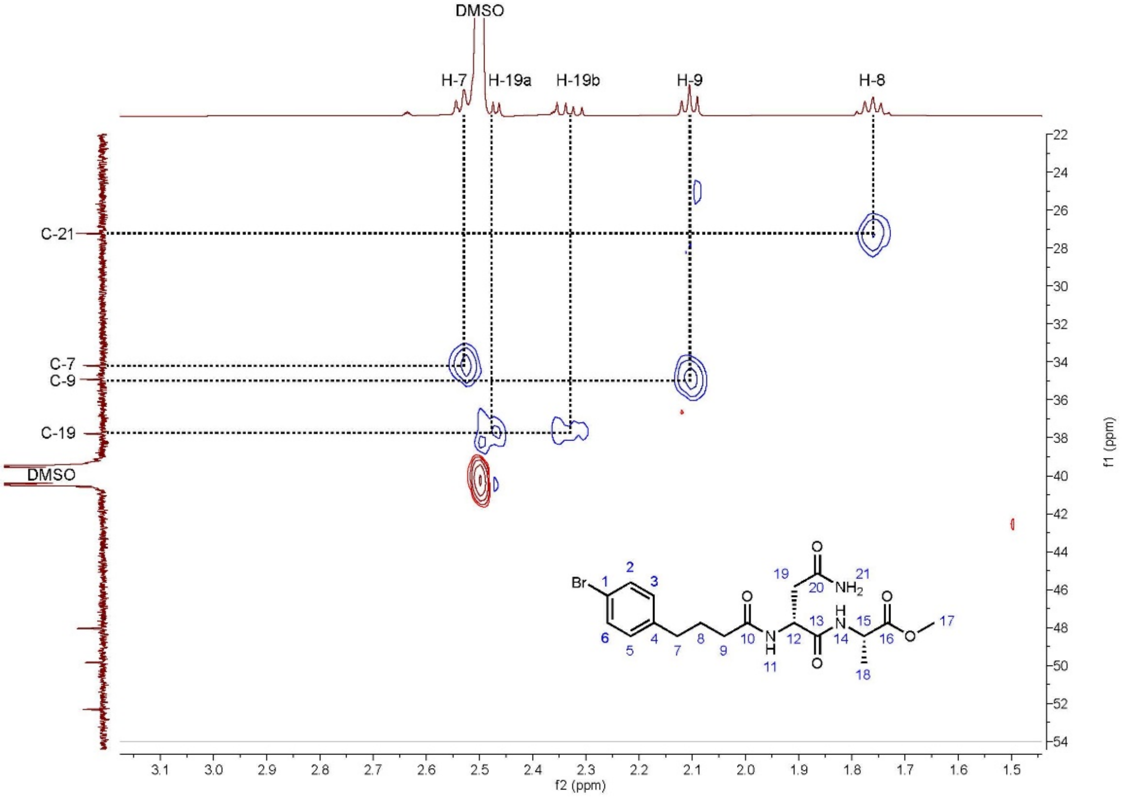

Supplementary References

1. Volpe, M.R. et al. A small molecule inhibitor prevents gut bacterial genotoxin production. *Nat Chem Biol*, in press (2022).

2. Park, H.B., Perez, C.E., Perry, E.K. & Crawford, J.M. Activating and Attenuating the Amicoumacin Antibiotics. *Molecules* **21**(2016).

3. Terekhov, S.S. et al. Ultrahigh-throughput functional profiling of microbiota communities. *Proc Natl Acad Sci U S A* **115**, 9551-9556 (2018).

4. Nougayrede, J.P. et al. *Escherichia coli* induces DNA double-strand breaks in eukaryotic cells. *Science* **313**, 848-51 (2006).

5. Putze, J. et al. Genetic structure and distribution of the colibactin genomic island among members of the family *Enterobacteriaceae*. *Infect Immun* **77**, 4696-703 (2009).

6. Sarshar, M. et al. Genetic diversity, phylogroup distribution and virulence gene profile of *pks* positive *Escherichia coli* colonizing human intestinal polyps. *Microb Pathog* **112**, 274-278 (2017).

7. Garcia-Gonzalez, E. et al. Biological effects of paenilamicin, a secondary metabolite antibiotic produced by the honey bee pathogenic bacterium *Paenibacillus larvae*. *Microbiologyopen* **3**, 642-56 (2014).

8. Park, D. et al. Genetic analysis of xenocoumacin antibiotic production in the mutualistic bacterium *Xenorhabdus nematophila*. *Mol Microbiol* **73**, 938-49 (2009).

9. Kevany, B.M., Rasko, D.A. & Thomas, M.G. Characterization of the complete zwittermicin A biosynthesis gene cluster from *Bacillus cereus*. *Appl Environ Microbiol* **75**, 1144-55 (2009).

10. Luo, Y. et al. Validation of the intact zwittermicin A biosynthetic gene cluster and discovery of a complementary resistance mechanism in *Bacillus thuringiensis*. *Antimicrob Agents Chemother* **55**, 4161-9 (2011).

11. Chen, W. et al. Draft genome sequence of *Brevibacillus brevis* strain X23, a biocontrol agent against bacterial wilt. *J Bacteriol* **194**, 6634-5 (2012).

12. Westman, E.L., Yan, M., Waglechner, N., Koteva, K. & Wright, G.D. Self resistance to the atypical cationic antimicrobial peptide edeine of *Brevibacillus brevis* Vm4 by the N-acetyltransferase EdeQ. *Chem Biol* **20**, 983-90 (2013).

13. Johnson, E.T., Bowman, M.J. & Dunlap, C.A. *Brevibacillus fortis* NRS-1210 produces edeines that inhibit the in vitro growth of conidia and chlamydospores of the onion pathogen *Fusarium oxysporum* f. sp. *cepae*. *Antonie Van Leeuwenhoek* **113**, 973-987 (2020).

14. Li, Y. et al. Directed natural product biosynthesis gene cluster capture and expression in the model bacterium *Bacillus subtilis*. *Sci Rep* **5**, 9383 (2015).

15. Reimer, D., Pos, K.M., Thines, M., Grun, P. & Bode, H.B. A natural prodrug activation mechanism in nonribosomal peptide synthesis. *Nat Chem Biol* **7**, 888-90 (2011).

16. Muller, S. et al. Paenilamicin: structure and biosynthesis of a hybrid nonribosomal peptide/polyketide antibiotic from the bee pathogen *Paenibacillus larvae*. *Angew Chem Int Ed Engl* **53**, 10821-5 (2014).